RSC Advances

PAPER

View Article Online
View Journal | View Issue

Cite this: *RSC Adv.*, 2019, **9**, 28636

A coumarin–dihydroperimidine dye as a fluorescent chemosensor for hypochlorite in 99% water†

Yasuhiro Shiraishi, * Chiharu Yamada and Takayuki Hirai

The hypochlorite anion (OCl^-), a reactive oxygen species (ROS), is an important microbicidal agent in the immune system. Accurate and selective detection of OCl^- in environmental and biological samples by a fluorescent molecular sensor is an important subject. All previously reported sensors, however, have suffered from tedious multi-step synthesis for the sensors and the use of large amounts of organic solvents for the analysis. Herein, we report that a coumarin–dihydroperimidine dye prepared by facile condensation behaves as a fluorescent sensor for OCl^- in 99% water. The sensor exhibits weak fluorescence, but OCl^--selective dehydrogenation of its dihydroperimidine unit creates a strong blue fluorescence. This turn-on fluorescence response facilitates selective and sensitive detection of OCl^- in the physiological pH range. *Ab initio* calculation revealed that the fluorescence enhancement by OCl^- is triggered by intramolecular proton transfer from the coumarin –OH to the imine nitrogen of the formed perimidine moiety.

Received 18th July 2019
Accepted 5th September 2019

DOI: 10.1039/c9ra05533a

rsc.li/rsc-advances

Introduction

Reactive oxygen species (ROS) play crucial roles in several life functions.[1] Among them, hypochlorous acid (HClO) is one of the most biologically important ROS.[2] HClO undergoes deprotonation at physiological pH and produces the hypochlorite anion (OCl^-),[3] which behaves as a microbicidal agent in the immune system.[4] OCl^- is produced *in vivo* by the reaction of hydrogen peroxide (H_2O_2) with Cl^- *via* an enzymatic reaction on myeloperoxidase (MPO).[5] Controlled generation of OCl^- is necessary to inhibit invading microbes. Uncontrolled OCl^- generation, however, causes several diseases such as neuron degeneration, arthritis, and cancer,[6] because OCl^- reacts with several biomolecules such as amino acids, proteins, and nucleosides.[7] In addition, HClO is widely used in daily life for sterilization and disinfection of water supplies, and high residual concentrations of OCl^- in water is hazardous to human and animal health.[8] Analytical methods that quantitatively detect small amount of OCl^- in environmental and biological samples on inexpensive instrumentations with simple pre-treatment are necessary.

Fluorometric analysis with OCl^--selective molecular sensors is one promising method for this purpose since this facilitates simple quantification or imaging of OCl^- with a common fluorescence spectrometer or microscope apparatus.[9] A number of fluorescent OCl^- sensors have been reported;[10–17] however, many of them require tedious multi-step procedures for the synthesis of sensors or a solution containing a large amount of organic solvents for sensing due to the low solubility of the sensors in water. Among the previously reported OCl^- sensors, a "dihydroperimidine"-based sensor designed by Goswami *et al.*[18] has the simplest structure, which can be prepared by a facile condensation. As shown in Scheme 1, they synthesized a naphthol–dihydroperimidine dye by the condensation of 1,8-diaminonaphthalene with 1-formyl-2-naphthol as a fluorophore. The sensor shows a sensitive turn-on fluorescence response *via* an OCl^--selective dehydrogenation of the dihydroperimidine unit. The sensor, however, requires a solution containing 60% MeCN owing to its low solubility in water. Based on this molecular design, Fan *et al.*[19] synthesized a sensor by the condensation of 1,8-diaminonaphthalene with 7-diethylamino-1,4-benzoxazin-2-one as a fluorophore. Although the sensor exhibits a selective and sensitive response towards OCl^-, it still requires a large amount of organic solvent (80%

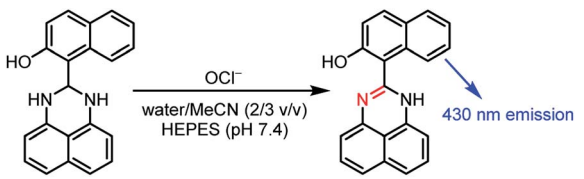

Scheme 1 A naphthol–dihydroperimidine dye exhibiting a turn-on fluorescence response toward OCl^-.[18]

Research Center for Solar Energy Chemistry, Division of Chemical Engineering, Graduate School of Engineering Science, Osaka University, Toyonaka 560-8531, Japan. E-mail: shiraish@cheng.es.osaka-u.ac.jp

† Electronic supplementary information (ESI) available: Table S1, Fig. S1–S10, and Cartesian coordinates for the molecules. See DOI: 10.1039/c9ra05533a

DMF) for the sensing. Design of a sensor that can be synthesized by a simple procedure and has a high water solubility is therefore desirable.

We used coumarin as a fluorophore due to its relatively high water solubility,[20] high fluorescence quantum yield,[21] large Stokes shift,[22] high stability,[23] and good cell permeability.[24] As shown in Scheme 2, the sensor **1**, synthesized by a simple condensation of 1,8-diaminonaphthalene with 8-formyl-7-hydroxy-4-methylcoumarin, is soluble in water containing only 1% organic solvents. The sensor shows a weak fluorescence, but OCl^--selective dehydrogenation of its dihydroperimidine unit creates a strong fluorescence at 462 nm. This turn-on response facilitates sensitive detection of OCl^-. Several spectroscopic analysis and *ab initio* calculations revealed that this turn-on response by OCl^- is triggered by intramolecular proton transfer from the coumarin –OH to the imine nitrogen of the formed perimidine unit.

Results and discussion

Synthesis and fluorescence properties of the sensor

The sensor **1** was prepared by the reaction shown in Scheme 2. 8-Formyl-7-hydroxy-4-methylcoumarin prepared by formylation of 7-hydroxy-4-methylcoumarin (yield: 45%)[25] and 1,8-diaminonaphthalene were dissolved in EtOH, and the solution was stirred at 80 °C for 2.5 h in an aerated condition. The solid formed was recovered by filtration and washed thoroughly with EtOH, affording **1** as pale pink solids with 69% yield (overall yield: 31%). The purity of **1** was confirmed by ^{1}H NMR, ^{13}C NMR and FAB-MS analysis (Fig. S1–S3, ESI†). **1** is soluble in common organic solvents such as DMSO, $CHCl_3$, DMF, and MeCN and in aqueous solutions with 1% organic solvents such as DMSO and MeCN. Fig. S4 (ESI†) shows the absorption spectra of 1% MeCN solutions containing different concentrations of **1**. The linear relationship between the absorbance at 325 nm and the concentration of **1** (0–20 μM) indicates that it follows the Beer's law, suggesting that **1** is fully soluble in the solutions. Note that the molar extinction coefficient of **1** at 325 nm was determined to be 10 039 M^{-1} cm^{-1}.

Fluorescence spectra of **1** (10 μM) were measured in a buffered water/MeCN mixture (99/1 v/v) with pH 7.0 (HEPES 0.1 M) at 25 °C (λ_{ex} = 344 nm). As shown in Fig. 1, **1** itself shows a very weak fluorescence (fluorescence quantum yield, Φ_F = 0.002). In contrast, addition of 50 equiv. of OCl^- to the solution followed by stirring for 20 min creates a strong blue fluorescence at 462 nm (Φ_F = 0.082). Other anions (F^-, Cl^-, AcO^-, NO_2^-, NO_3^-, ClO_4^-, and HSO_4^-), ROS [hydroxyl radical (·OH), singlet oxygen ($^1O_2$), H_2O_2, superoxide radical ($\cdot O_2^-$), and *tert*-butyl hydroperoxide (*t*-BuOOH)], or RNS [NO and peroxynitrite ($ONOO^-$)], when added to the solution containing **1**, scarcely change the fluorescence spectra, indicating that OCl^- selectively triggers fluorescence enhancement of **1**.

Fig. 2a shows the results of fluorescence titration of **1** with OCl^-. Stepwise addition of OCl^- increases the intensity of the 462 nm fluorescence. As shown in Fig. 2b, the change in the ratio of fluorescence intensity at 462 nm (FI/FI_0) with the OCl^- concentrations clearly shows linear relationship, indicating that **1** facilitates accurate OCl^- sensing at ~100 μM. The lower detection limit was determined to be 3.3 μM based on the signal-to-noise (S/N) ratio using the equation ($DL = 3 \times SD/S$),[26] where SD is the standard deviation of blank analysis (SD = 0.19, n = 10) and S is the slope of the fluorescence intensity *versus* the OCl^- concentrations (S = 0.18 μM^{-1}). This detection limit (3.3 μM) is lower than the physiological OCl^- concentrations (5–25 μM) in the human body,[27] suggesting that **1** facilitates sensitive OCl^- detection even in high-water-content solution.

Reaction of the sensor with OCl^-

As shown in Scheme 2, the turn-on fluorescence response of **1** upon addition of OCl^- is triggered by the transformation to **1′**, *via* dehydrogenation of the dihydroperimidine moiety of **1**. This transformation is confirmed by ^{1}H, ^{13}C NMR and FAB-MS analysis of a DMSO-d_6 solution containing **1** and OCl^- (Fig. S5–S7, ESI†). Partial ^{1}H NMR charts of **1** and **1′** measured in DMSO-d_6 are shown in Fig. 3, where the 2D COSY spectra were used for the assignment of the respective chemical shifts

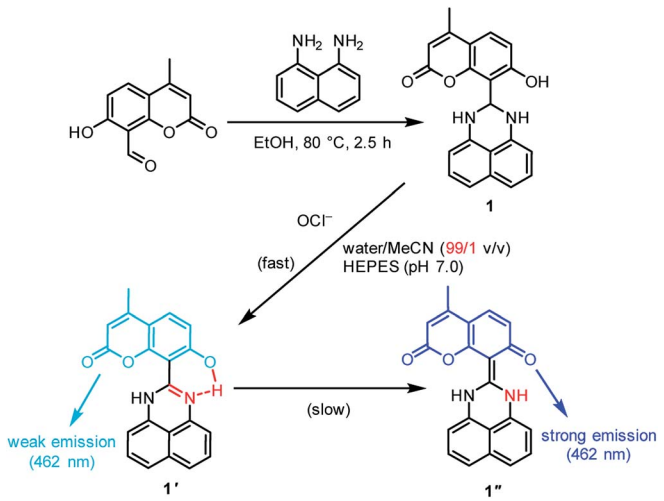

Scheme 2 Synthesis of the sensor **1**, and proposed mechanism for selective turn-on fluorescence response by OCl^-.

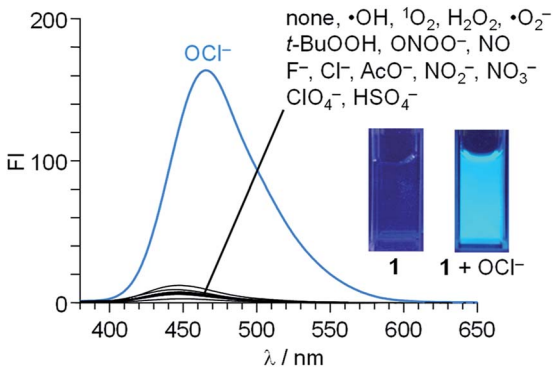

Fig. 1 Fluorescence spectra (λ_{ex} = 344 nm) of **1** (10 μM) in a buffered water/MeCN mixture (99/1 v/v; HEPES 0.1 M, pH 7.0) at 25 °C with 50 equiv. of each respective analytes. All spectra were obtained after stirring the solution for 20 min.

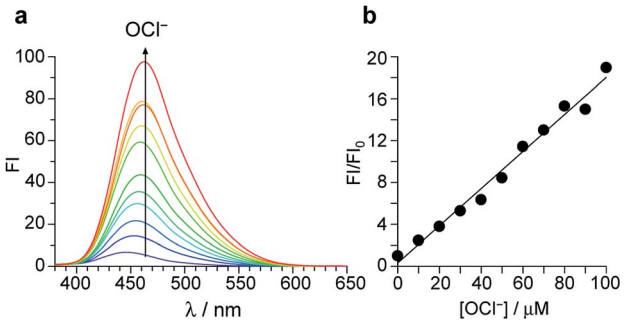

Fig. 2 (a) Change in fluorescence spectra of **1** (10 μM) upon titration with OCl^- in a buffered water/MeCN mixture (99/1 v/v; HEPES 0.1 M, pH 7.0) at 25 °C. (b) Change in the ratio of fluorescence intensity at 462 nm (FI/FI_0) *versus* the OCl^- concentration. The respective data were obtained after stirring the solution for 20 min.

(Fig. S8 and S9, ESI†). As shown in Fig. 3a, **1** shows an H^a proton at the 2-position of the dihydroperimidine unit at 6.0 ppm. However, as shown in Fig. 3b, addition of OCl^- to the solution leads to almost complete disappearance of the H^a proton. In addition, **1** shows two N–H protons of the dihydroperimidine moiety at 7.0 ppm. After the addition of OCl^-, its chemical shift moves to 7.1 ppm, and its integral value becomes almost 1. These data indicate that H^a and one N–H proton of **1** are removed by the reaction with OCl^-. The dehydrogenation of **1** by OCl^- is confirmed by FAB-MS analysis. As shown in Fig. S3 (ESI†), **1** shows a peak at *m*/*z* 344.1 assigned to $[\mathbf{1}]^+$. In contrast, as shown in Fig. S7 (ESI†), a solution containing **1** and OCl^-

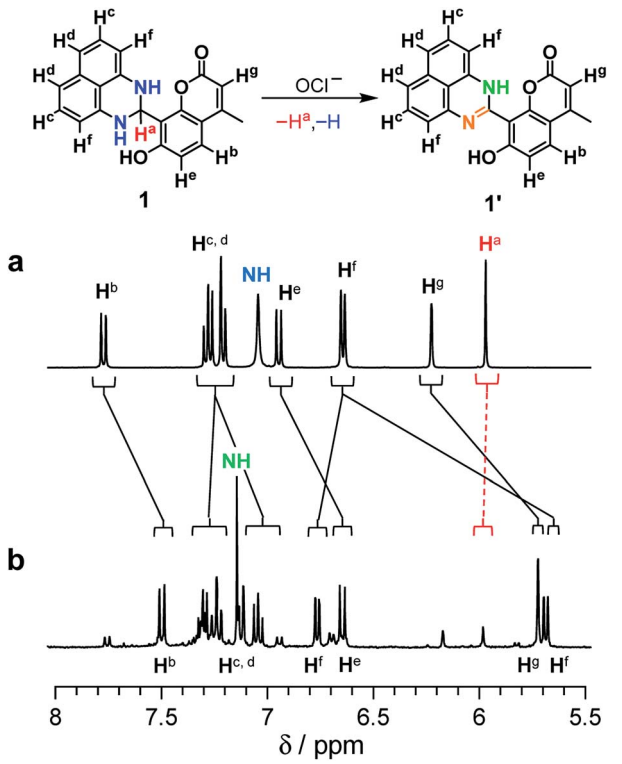

Fig. 3 ^1H NMR chart of **1** (24 mM) measured in DMSO-d_6 (a) without and (b) with 8 equiv of OCl^- (400 MHz, 30 °C).

shows a peak at *m*/*z* 342.1 assigned to the dehydrogenated product $[\mathbf{1}']^+$. These NMR and FAB-MS data clearly suggest that dehydrogenation of the dihydroperimidine moiety of **1** *via* the oxidation by OCl^- gives **1′** containing the perimidine moiety.

As shown in Scheme 2, the enol–imine form (**1′**) is rapidly produced by dehydrogenation of **1** by OCl^- and shows a weak fluorescence ($\Phi_F = 0.009$). Then, **1′** undergoes tautomerization to the keto-amine form (**1″**) *via* a proton transfer of the coumarin –OH to the imine nitrogen of the perimidine unit, as often observed for similar *o*-hydroxyl Schiff bases,[28,29] and exhibits a strong fluorescence ($\Phi_F = 0.082$). This sequence is confirmed by time-dependent changes in the absorption and fluorescence spectra of **1** monitored after addition of OCl^-. As shown in Fig. 4a, addition of OCl^- immediately increases the fluorescence intensity at 462 nm within 1 min (blue to red line), although the intensity is weak. Then, the intensity gradually increases with time and plateaus after 15 min, creating a strong fluorescence, where the emission wavelengths scarcely change during the measurements. This indicates that the reaction of **1** with OCl^- creates two different emitting species. As shown in Fig. 4b, absorption spectrum of **1** also changes immediately after the OCl^- addition within 1 min (blue to red line). Then, the spectrum changes gradually with a decrease in *ca.* 320 nm absorbance and an increase in *ca.* 375 nm absorbance. The isosbestic point at 344 nm clearly indicates that, as shown in Scheme 2, the reaction of **1** with OCl^- rapidly produces

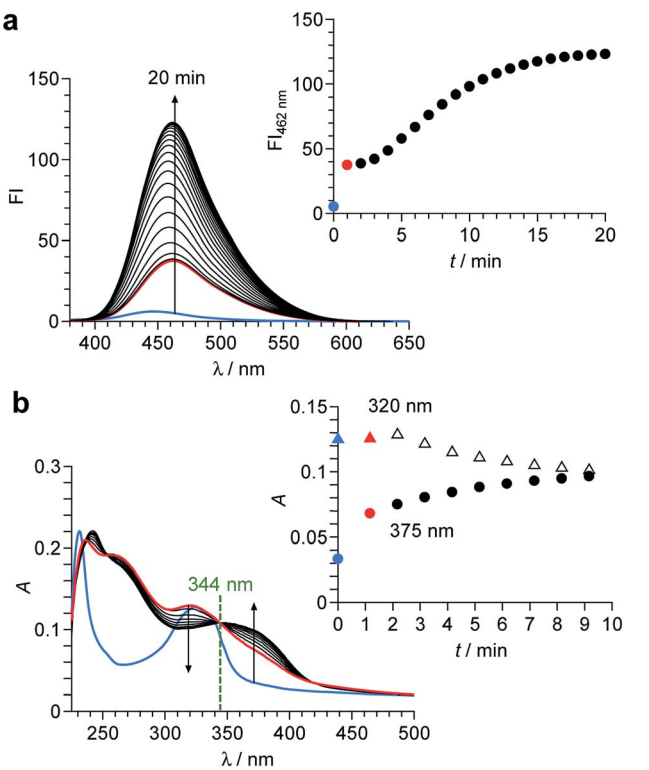

Fig. 4 (a) Time-dependent change in fluorescence spectra ($\lambda_{ex} = 344$ nm) of **1** (10 μM) in a buffered water/MeCN mixture (99/1 v/v; HEPES 0.1 M, pH 7.0) at 25 °C after addition of 50 equiv. of OCl^-. The inset shows change in the intensity at 462 nm. (b) Time-dependent change in absorption spectra of **1** after addition of 50 equiv. of OCl^-. The inset shows change in the absorbance at 320 nm and 375 nm.

a weakly-fluorescent enol-imine form (**1′**) and its slow tautomerization by the intramolecular proton transfer creates a strongly-fluorescent keto-amine form (**1″**).

The tautomerization of **1′** to **1″** is promoted by polar water molecules. It is well known that, for the tautomerization of *o*-hydroxy Schiff bases,[30,31] the enol-imine form is stabilized in less polar solvents such as benzene, while the keto-amine form is stable in polar solvents such as EtOH. Fig. S10 (ESI†) shows the change in fluorescence intensity of **1** after addition of OCl^- in MeCN solutions with different water contents. In all solutions, the weakly-fluorescent enol-imine form (**1′**) is rapidly produced by the addition of OCl^-. The strongly-fluorescent keto-amine form (**1″**) is not produced in low-water-content solutions (30% and 60%), whereas increasing the water content produces **1″**. This indicates that increasing water content increases the polarity of solutions and promotes **1′**-to-**1″** tautomerization. However, as shown in Fig. 3b and S5–S7 (ESI†), ^1H, ^{13}C NMR and FAB-MS analysis of the product obtained by the reaction of **1** with OCl^- in DMSO-d_6 detected **1′**. This is because the **1′**-to-**1″** tautomerization is not promoted in less polar DMSO. These findings clearly support the **1** → **1′** → **1″** transformation by the reaction of **1** with OCl^- in high-water-content solutions, as shown in Scheme 2.

Ab initio calculations

The mechanism for the turn-on fluorescence response of **1** was clarified by *ab initio* calculations. The structures and optical properties of **1**, **1′**, and **1″** species were calculated by the density functional theory (DFT) and the time-dependent DFT (TD-DFT), respectively, within the Gaussian 03 program with water as a solvent. As summarized in Table S1 (ESI†), singlet electronic transition of **1** mainly consists of HOMO → LUMO+2 (S_0 → S_4) transition. Its calculated transition energy (3.76 eV, 330 nm) is close to the absorption maximum (λ_{max}) of **1** at 323 nm (Fig. 4b, blue line). As shown in Fig. 5 (left), π-electrons of both HOMO and LUMO+2 of **1** are localized on the dihydroperimidine moiety, indicating that photoexcitation of the coumarin fluorophore is not populated. This therefore results in almost no fluorescence of **1**.

As shown in Fig. 5 (center), optimized structure of **1′** has a planar structure, where the coumarin and perimidine units lie on the same plane. It is noted that the structural optimization spontaneously creates an H-bonding interaction between the imine nitrogen and coumarin –OH units, in which the N–O distance of ~2.5 Å indicates strong electrostatic interaction between these units.[32] The structural regulation by the H-bonding may create the planer structure. As shown in Table S1 (ESI†), the electronic transition of **1′** mainly consists of HOMO-1 → LUMO+1 (S_0 → S_6) transition. Its energy (3.97 eV, 312 nm) is also close to that for the absorption maximum (320 nm) of **1′** (Fig. 4b, red line). As shown in Fig. 5 (center), relatively large distribution of π-electrons are observed on both HOMO-1 and LUMO+1 for **1′**. This is because the H-bonding interaction of the coumarin –OH increases the electron density of coumarin unit.[33] The enhanced photoexcitation of the coumarin units may therefore result in weak fluorescence of **1′**.

As shown in Fig. 5 (right), optimized structure of **1″** also has a planar structure owing to the C=C bond formation between the coumarin and dihydroperimidine units. Singlet electronic transition of **1″** is mainly contributed by HOMO-1 → LUMO+1 (S_0 → S_4) transition (Table S1, ESI†). Its transition energy (3.64 eV, 340 nm) is also close to that for the absorption band (375 nm) of **1″** (Fig. 4b). As shown in Fig. 5 (right), almost all of the π-electrons of both HOMO-1 and LUMO+1 for **1″** are localized on the coumarin units because complete deprotonation of the coumarin –OH significantly increases the electron density of

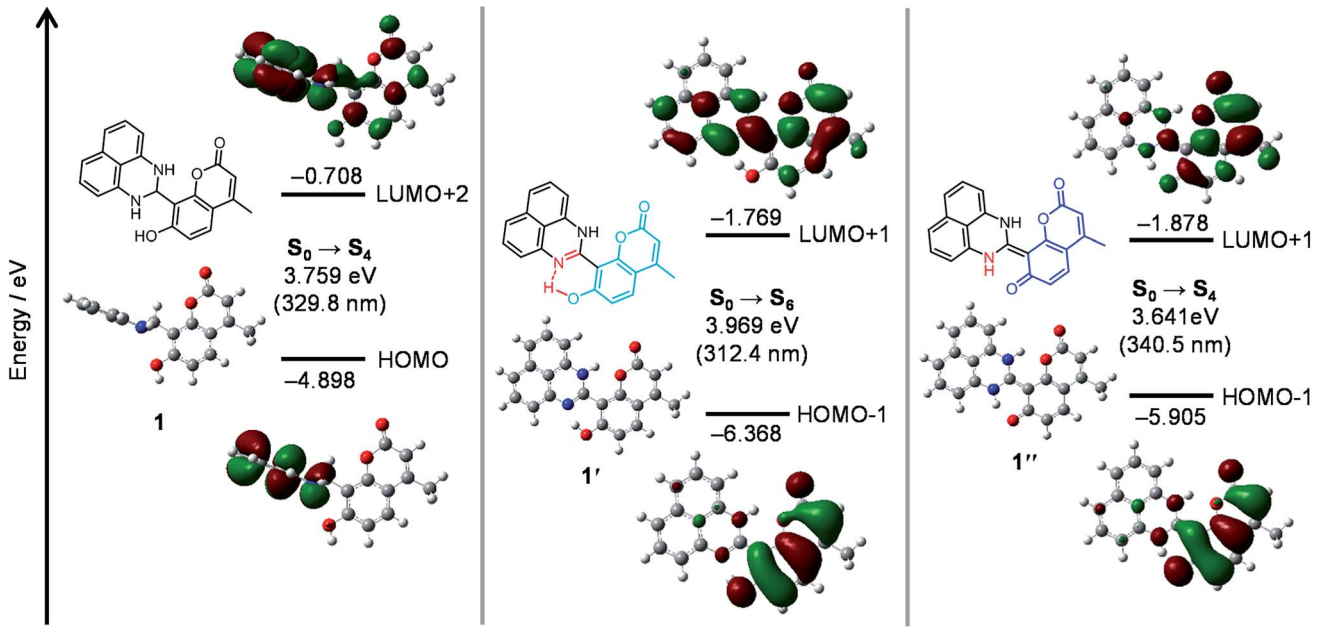

Fig. 5 Energy diagrams and interfacial plots of main molecular orbitals of (left) **1**, (center) **1′** and (right) **1″**, calculated at the DFT level (B3LYP/6-31+G*).

the coumarin unit.[33] This therefore results in strong coumarin fluorescence from **1″**.

The total energies of **1′** and **1″** in water were determined to be −717846.94 and −717850.01 kcal mol^{-1}, respectively. The lower energy of **1″** (ΔE = 3.07 kcal mol^{-1}) indicates that the keto-amine form (**1″**) is indeed more stable in water than the enol-imine form (**1′**). This further supports the **1** → **1′** → **1″** transformation by the reaction of **1** with OCl^- in high-water-content solutions. These DFT results clearly indicate that the dihydroperimidine unit acts as a proton acceptor for the coumarin –OH (Scheme 2). The OCl^--triggered formation of the perimidine unit leads to H-bonding interaction between the imine nitrogen and coumarin –OH and creates weak emission (**1′**). Water-assisted tautomerization of **1′** to **1″** leads to complete proton transfer from the coumarin –OH and creates strong emission (**1″**).

Effect of pH

It is noted that pH of the solution is critical for the OCl^- sensing. Fig. 6 shows the fluorescence intensity of **1** at 462 nm measured at different pH with and without 50 equiv. of OCl^-, where the mole fraction distributions of Cl_2, HClO, and OCl^- are also shown based on their equilibria in water,[34,35] using the following equations:

$$Cl_2 + H_2O \rightleftharpoons HClO + H^+ + Cl^- \ (pK_a = 1.4) \quad (1)$$

$$HClO \rightleftharpoons ClO^- + H^+ \ (pK_a = 7.6) \quad (2)$$

The fluorescence enhancement of **1** by OCl^- occurs at neutral physiological pH (6–8), and does not occur at acidic or basic pH. In acidic media (pH < 6), protonation of OCl^- (HClO formation; eqn (2)) cancels the basicity of OCl^- and, hence, suppresses dehydrogenation of the dihydroperimidine unit of **1**. In contrast, basic media (pH > 8) stabilize OCl^-, but the fluorescence enhancement does not occur. This is probably because, as observed for several OCl^- sensors,[10,14,15] the oxidation ability of OCl^- decreases in basic media and inhibits dehydrogenation of the dihydroperimidine unit. These data suggest that **1** facilitates fluorometric sensing of OCl^- in physiological pH media (pH 6–8).

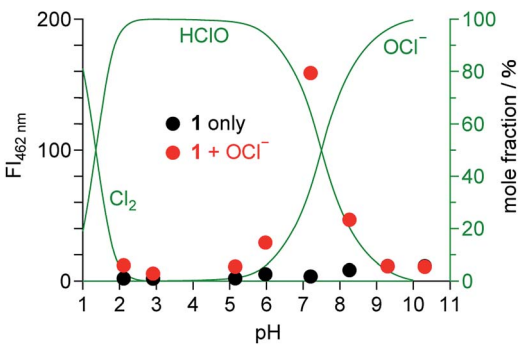

Fig. 6 Fluorescence intensity of **1** (10 μM) monitored at 462 nm in water/MeCN mixtures (99/1 v/v) at 25 °C with different pH, (red) with and (black) without OCl^- (50 equiv.). The mole fraction distributions of Cl_2, HClO, and OCl^- calculated based on the equilibria (eqn (1) and (2)) are shown by green lines.

Conclusions

We synthesized a coumarin–dihydroperimidine dye (**1**), acting as a fluorescent sensor for OCl^- in 99% water. **1** shows a weak fluorescence, but OCl^--selective dehydrogenation of its dihydroperimidine unit creates a strong blue fluorescence. **1** facilitates selective and sensitive OCl^- detection at physiological pH. The turn-on response of **1** occurs *via* two-step reactions. The dehydrogenation by OCl^- rapidly produces the enol-imine form (**1′**) involving the H-bonding interaction between the imine nitrogen and coumarin –OH. This increases the electron density of the coumarin unit, resulting in weak fluorescence. **1′** undergoes tautomerization to the keto-amine form (**1″**) due to the stabilization in polar water media. The complete proton transfer from the coumarin –OH to the imine nitrogen significantly increases the electron density of the coumarin unit, exhibiting a strong fluorescence. The molecular design based on the dihydroperimidine unit as an OCl^--driven proton sensor, may contribute to the design of efficient fluorescent sensors for OCl^- in environmental and biological samples.

Experimental

General

All chemicals were used as received. ·OH was generated by the Fenton reaction.[36] $^1O_2$ was generated from the H_2O_2/MoO_4^{2-} system in alkaline media.[37] NO was generated using sodium nitroferricyanide(III) dehydrate.[38] $ONOO^-$ was generated from the SIN-1 reagent (Dojindo Molecular Technologies, Japan). $\cdot O_2^-$ was generated using potassium superoxide (KO_2).[36] Fluorescence spectra were measured on a JASCO FP-6500 fluorescence spectrophotometer with a 10 nm path length cell (both excitation and emission slit widths, 5.0 nm) at 298 ± 1 K using a temperature controller.[39] Absorption spectra were measured on an UV-visible photodiode-array spectrometer (Shimadzu; Multispec-1500) equipped with a temperature controller (S-1700).[40] All measurements were performed under aerated conditions. ^{1}H and ^{13}C NMR charts were obtained using a JEOL JNM-ECS400 spectrometer. FAB-MS analysis was performed on a JEOL JMS 700 Mass Spectrometer. Fluorescence quantum yields (Φ_F) were determined with quinine sulfate dihydrate (in 0.1 M $HClO_4$ solution) as a standard.[41,42]

Synthesis of the sensor (1) [8-(2,3-dihydro-1*H*-perimidin-2-yl)-7-hydroxy-4-methyl-2*H*-chromen-2-one]

8-Formyl-7-hydroxy-4-methylcoumarin (200 mg, 0.98 mmol)[25] and 1,8-diaminonaphthalene (188 mg, 1.20 mmol) were dissolved in EtOH (20 ml), and the solution was stirred at 80 °C for 2.5 h. The solid formed was recovered by filtration and washed thoroughly with EtOH, affording **1** as pale pink solids. Yield: 234.4 mg (69.4%). ^{1}H NMR (400 MHz, DMSO-d_6, TMS), δ (ppm): 10.38 (1H, s), 7.74 (1H, d, J = 8.8 Hz), 7.24–7.28 (2H, m), 7.18–

7.20 (2H, m), 7.03 (2H, s), 6.94 (1H, d, $J = 8.8$ Hz), 6.64 (2H, d, $J = 7.2$ Hz), 6.23 (1H, s), 5.99 (1H, s), 2.44 (3H, s). ^{13}C NMR (100 MHz, DMSO-d_6, TMS), δ (ppm): 161.0, 159.6, 153.8, 152.4, 142.9, 134.2, 126.9, 126.7, 117.2, 113.5, 113.2, 112.0, 110.9, 110.3, 106.3, 59.9, 55.9, 18.3. FAB-MS: *m*/*z*: calcd for $C_{21}H_{16}O_3N_2^+$ (M^+) 344.1161; found (ESI†): 344.1158.

Calculation details

Ab initio calculations were performed with tight convergence criteria at the DFT level within the Gaussian 03 package, using the B3LYP/6-31+G(D) basis set for all atoms. The excitation energies and oscillator strengths of the compounds were calculated by TDTFT[43] at the same level of optimization using the PCM with water as a solvent.[44] Cartesian coordinates are summarized at the end of ESI.†

Conflicts of interest

There are no conflicts to declare.

Acknowledgements

This work was supported by the Grant-in Aid for Scientific Research (No.15K06556) from the Ministry of Education, Culture, Sports, Science and Technology, Japan (MEXT).

Notes and references

1 A. Manke, S. Luanpitpong, C. Dong, L. Wang, X. He, L. Battelli, R. Derk, T. A. Stueckle, D. W. Porter, T. Sager, H. Gou, C. Z. Dinu, N. Wu, R. R. Mercer and Y. Rojanasakul, *Int. J. Mol. Sci.*, 2014, **15**, 7444.
2 A. Gomes, E. Fernandes and J. L. F. C. Lima, *J. Biochem. Biophys. Methods*, 2005, **65**, 45.
3 J. Shepherd, S. A. Hilderbrand, P. Waternan, J. W. Heinecke, R. Weissleder and P. Libby, *Chem. Biol.*, 2007, **14**, 1221.
4 A. J. Kettle and C. C. Winterbourn, *Redox Rep.*, 1997, **3**, 3.
5 T. Aoki and M. Munemori, *Anal. Chem.*, 1983, **55**, 209.
6 T. Sugiyama, M. Fujita, N. Koide, I. Mori, T. Yoshida, H. Mori and T. Yokochi, *Microbiol. Immunol.*, 2004, **48**, 957.
7 S. L. Hazen, F. F. Hsu, K. Duffin and J. W. Heinecke, *J. Biol. Chem.*, 1996, **271**, 23080.
8 L. C. Adam and G. Gordon, *Anal. Chem.*, 1995, **67**, 535.
9 Q. Xu, K.-A. Lee, S. Lee, K. M. Lee, W.-J. Lee and J. Yoon, *J. Am. Chem. Soc.*, 2013, **135**, 9944.
10 J. Xu, H. Yuan, C. Qin, L. Zeng and G.-M. Bao, *RSC Adv.*, 2016, **6**, 107525.
11 L. Long, Y. Wu, L. Wang, A. Gong, F. Hu and C. Zhang, *Chem. Commun.*, 2015, **51**, 10435.
12 L. Long, D. Zhang, X. Li, J. Zhang, C. Zhang and L. Zhou, *Anal. Chim. Acta*, 2013, **775**, 100.
13 Y.-R. Zhang, X.-P. Chen, J. Shao, J.-Y. Zhang, Q. Yuan, J.-Y. Miao and B.-X. Zhao, *Chem. Commun.*, 2014, **50**, 14241.
14 Y. Huang, Y. Zhang, F. Huo, J. Chao and C. Yin, *Sens. Actuators, B*, 2019, **287**, 453.
15 J. Zha, B. Fu, C. Qin, L. Zeng and X. Hu, *RSC Adv.*, 2014, **4**, 43110.
16 K. Wang, P. Sun, X. Chao, D. Cao, Z. Mao and Z. Liu, *RSC Adv.*, 2018, **8**, 6904.
17 J.-T. Hou, H. S. Kim, C. Duan, M. S. Ji, S. Wang, L. Zeng, W. X. Ren and J. S. Kim, *Chem. Commun.*, 2019, **55**, 2533.
18 S. Goswami, A. Manna, S. Paul, C. K. Quah and H.-K. Fun, *Chem. Commun.*, 2013, **49**, 11656.
19 J. Fan, H. Mu, H. Zhu, J. Wang and X. Peng, *Analyst*, 2015, **140**, 4594.
20 J. Li, C.-F. Zhang, Z.-Z. Ming, G.-F. Hao, W.-C. Yang and G.-F. Yang, *Tetrahedron*, 2013, **69**, 4743.
21 C. M. Krauter, J. Mohring, T. Buckup, M. Pernpointner and M. Motzkus, *Phys. Chem. Chem. Phys.*, 2013, **15**, 17846.
22 L. Yuan, W. Lin, Y. Yang, J. Song and J. Wang, *Org. Lett.*, 2011, **13**, 3730.
23 Y. Feng, Y. Yang, Y. Wang, F. Qiu, X. Song, X. Tang, G. Zhang and W. Liu, *Sens. Actuators, B*, 2019, **288**, 27.
24 J. Li, C.-F. Zhang, S.-H. Yang, W.-C. Yang and G.-F. Yang, *Anal. Chem.*, 2014, **86**, 3037.
25 X. Huang, Y. Dong, Q. Huang and Y. Cheng, *Tetrahedron Lett.*, 2013, **54**, 3822.
26 N. Sharma, S. I. Reja, V. Bhalla and M. Kumar, *Dalton Trans.*, 2014, **43**, 15929.
27 M. C. Mancini, B. A. Kairdolf, A. M. Smith and S. Nie, *J. Am. Chem. Soc.*, 2008, **130**, 10836.
28 C. Albayrak, G. Kastas, M. Odabasoglu and R. Frank, *Spectrochim. Acta, Part A*, 2013, **114**, 205.
29 H. Dal, Y. Suzen and E. Sahin, *Spectrochim. Acta, Part A*, 2007, **67**, 808.
30 H. Dal, *Asian J. Chem.*, 2014, **26**, 2759.
31 G. Kastas, *J. Mol. Struct.*, 2012, **1017**, 38.
32 G. A. Jeffrey, *An introduction to hydrogen bonding*, Oxford University Press, New York, 1997.
33 H. Zhi, J. Wang, S. Wang and Y. Wei, *J. Spectrosc.*, 2013, **2013**, 147128.
34 M. Whiteman and J. P. E. Spencer, *Biochem. Biophys. Res. Commun.*, 2008, **371**, 50.
35 S. Nakagawara, T. Goto, M. Nara, Y. Ozawa, K. Hotta and Y. Arata, *Anal. Sci.*, 1998, **14**, 691.
36 K. Setsukinai, Y. Urano, K. Kakinuma, H. J. Majima and T. Nagano, *J. Biol. Chem.*, 2003, **278**, 3170.
37 N. Umezawa, K. Tanaka, Y. Urano, K. Kikuchi, T. Higuchi and T. Nagano, *Angew. Chem., Int. Ed.*, 1999, **38**, 2899.
38 Z.-N. Sun, F.-Q. Liu, Y. Chen, P. K. H. Tam and D. Yang, *Org. Lett.*, 2008, **10**, 2171.
39 Y. Shiraishi, M. Nakamura, K. Yamamoto and T. Hirai, *Chem. Commun.*, 2014, **50**, 11583.
40 Y. Shiraishi, K. Tanaka, E. Shirakawa, Y. Sugano, S. Ichikawa, S. Tanaka and T. Hirai, *Angew. Chem., Int. Ed.*, 2013, **52**, 8304.
41 C. Wurth, M. Grabolle, J. Pauli, M. Spieles and U. R. -Genger, *Anal. Chem.*, 2011, **83**, 3431.
42 B. Bag and P. K. Bharadwaj, *J. Phys. Chem. B*, 2005, **109**, 4377.
43 R. E. Stratmann, G. E. Scuseria and M. J. Frisch, *J. Chem. Phys.*, 1998, **109**, 8218.
44 M. Cossi, V. Barone, R. Cammi and J. Tomasi, *Chem. Phys. Lett.*, 1996, **255**, 327.